American Mineralogist, Volume 79, pages 353–369, 1994

Chlorine, fluid immiscibility, and degassing in peralkaline magmas from Pantelleria, Italy

JACOB B. LOWENSTERN*
Mineral Resources Department, Geological Survey of Japan, 1-1-3 Higashi, Tsukuba, Ibaraki 305, Japan

ABSTRACT

This paper documents immiscibility among vapor, highly saline liquid, and silicate melt during the crystallization of peralkaline rhyolites from Pantelleria, Italy, prior to their eruption. Experiments conducted in a muffle furnace and with a high-temperature heating stage revealed three major types of silicate melt inclusions trapped in quartz phenocrysts. After entrapment in the host phenocryst, type I inclusions contained silicate melt. Type II inclusions contained silicate melt + hydrosaline melt (~60–80 wt% NaCl equivalent), and type III inclusions contained silicate melt + H_2O-CO_2 vapor. Two inclusions contained all three immiscible fluids: vapor, hydrosaline melt, and silicate melt. Fluid inclusions within outgassed matrix glass, viewed at room temperature, are interpreted as the crystallized equivalents of the hydrosaline melts within type II inclusions. These inclusions, 2–10 μm in size, consist of a bubble typically surrounded by a spherical shell of halite.

The presence of both vapor and hydrosaline melt in the magma indicates that the pantellerite was saturated with subcritical NaCl-H_2O fluids. At a given temperature and pressure, the fixed activity of Cl in these two fluids determines the activity and concentration of Cl in the silicate melt. The high concentrations of Cl in these pantellerites (~9000 ppm) are thus a function of the low activity coefficient for NaCl in pantellerite relative to metaluminous silicate liquids. The Cl contents of Pantellerian rhyolites indicate equilibration at pressures between 50 and 100 MPa. The high Cl contents of outgassed pantellerites may be due to minimal loss of HCl (not NaCl) during eruption, as compared with metaluminous rhyolites, which exsolve more HCl-rich vapors.

Discrepancies between the results of heating-stage experiments and longer muffle-furnace experiments indicate that measurements of melting and homogenization temperatures of melt inclusions may not be accurate unless sufficient time (>1 h) is allowed for equilibration at magmatic temperatures.

INTRODUCTION

Experimental studies show that the NaCl-H_2O system is characterized by immiscibility under a wide range of pressures and temperatures in the shallow crust (Sourirajan and Kennedy, 1962; Bodnar et al., 1985; Chou, 1987). Furthermore, research on the silicate melt–H_2O–alkali chloride ternary indicates that the Cl and H_2O contents of many magmas are sufficient to saturate the melt with immiscible vapor and liquid (hydrosaline melt) phases (Shinohara et al., 1989; Malinin et al., 1989; Metrich and Rutherford, 1992; Webster, 1992a). Evidence for immiscibility between silicate and H_2O-NaCl fluids is widespread in fluid inclusions found in phenocrysts of intrusive igneous bodies such as granites, syenites, and porphyry ore deposits (Roedder, 1972, 1984, 1992; Roedder and Coombs, 1967; Frost and Touret, 1989; Hansteen, 1989; Frezzotti, 1992). Some silicate melts show evidence for saturation with both vapor and hydrosaline melt (e.g., Frost and Touret, 1989). Because NaCl-H_2O fluids are precursors to ore-forming hydrothermal solutions, it is important to determine the factors that control their evolution and composition. Volcanic rocks are ideal for such studies because they contain quenched matrix and glass inclusions that can preserve the concentrations of magmatic volatiles during preeruptive degassing.

Studies of fluid inclusions in phenocryst-poor volcanic rocks have only rarely been undertaken. This stems, in part, from the scarcity of fluid inclusions in volcanic rocks (Tuttle, 1952), despite the oft-repeated conclusion that many igneous systems are fluid-saturated during crystallization and prior to eruption (Newman et al., 1988; Anderson et al., 1989; Luhr, 1990; Lowenstern et al., 1991; Lowenstern, 1993). Of the handful of studies of coexisting fluid and melt inclusions in volcanic systems, several have focused on rhyolites from Pantelleria, Italy. Abstracts by Clocchiatti et al. (1990) and Solovova et al. (1991) re-

* Present address: U.S. Geological Survey, M.S. 910, 345 Middlefield Road, Menlo Park, California 94025, U.S.A.

0003–004X/94/0304–0353$02.00

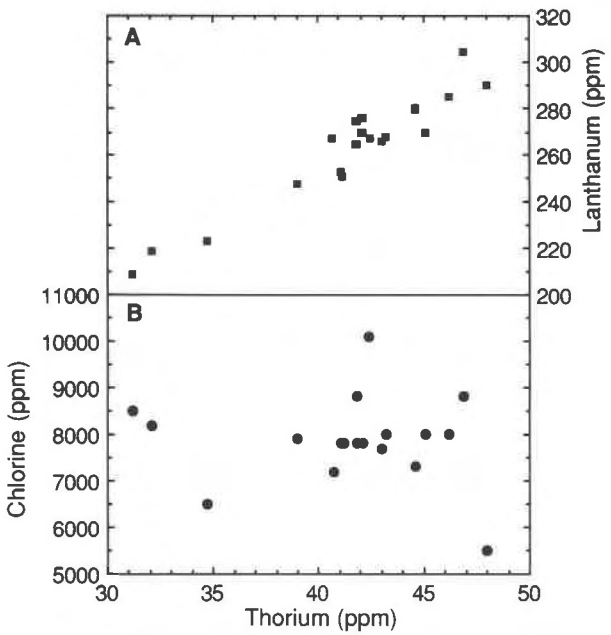

Fig. 1. Trace-element trends for glassy, unaltered Pantellerian rhyolites with an agpaitic index >1.75. (**A**) Relatively incompatible elements Th and La (distribution coefficient between bulk crystal and melt <0.01 and ~0.1, respectively; Mahood and Stimac, 1990) increase sympathetically during fractionation. (**B**) Cl concentrations do not correlate with indices of differentiation such as Th. Th and La data by INAA, Cl by specific ion electrode (G.A. Mahood, unpublished data). All analyses performed on whole rocks and glass separates; Cl contents may have been lowered slightly by syneruptive outgassing. Uncertainties (2σ) are approximately the size of the data points.

ported finding hydrosaline melts within silicate-melt inclusions from this locality. Lowenstern et al. (1991) showed that CO_2- and Cu-bearing vapor bubbles were also present in some melt inclusions. De Vivo et al. (1992) found fluid inclusions of a presumed magmatic vapor phase in syenite nodules ejected during eruption. Kovalenko et al. (1993) observed salt clusters within outgassed pantellerite glass and concluded that the erupting pantellerite was saturated with both vapor and salt-rich (hydrosaline) melt.

In this report, I corroborate the findings of this earlier research on pantellerites and elaborate upon them by documenting immiscibility among hydrosaline melts, low-density vapors, and silicate melts at high temperature and pressure. Seventy-nine silicate-melt inclusions in 28 phenocrysts were observed during 1-atm experiments using a high-temperature heating stage to record their behavior upon heating, consequent pressurization, and melting (Clocchiatti, 1972, 1975; Benhamou and Clocchiatti, 1976; Clocchiatti et al., 1990; Solovova et al., 1991; Frezzotti, 1992). This technique allows collection of photographic evidence and thermometric data about melt inclusions and the fluids trapped within them. As shown below, one can then evaluate both the effects of fluid immiscibility and subsequent degassing on the behavior and distribution of Cl in volcanic systems. Additionally, this paper attempts to explain the behavior of melt inclusions during cooling in nature and in the laboratory, permitting greater insight into petrologic and volcanologic processes.

Pantellerites, Cl, and melt inclusions

Pantelleria is a volcanic island that sits astride a drowned continental rift in the Strait of Sicily, between Sicily and Tunisia. The central part of the island is composed predominantly of pantellerites and associated trachytes and pantelleritic trachytes, though basalts are common on the island periphery (Civetta et al., 1984; Mahood and Hildreth, 1986). The island is the type locality of pantellerites, which are quartz-normative peralkaline rhyolites having agpaitic indices [A.I.: molar $(Na_2O + K_2O)/Al_2O_3$] commonly >1.75 (Macdonald and Bailey, 1973). Pantellerites are notable for their unusually high concentrations of total Fe (i.e., FeO_{tot} ~ 8%) and trace elements such as Zr, Nb, La, Hf, Zn, Mo, Rb, and Th. They have among the highest Cl contents of any igneous rocks on Earth, some samples reaching over 1 wt% (Kovalenko et al., 1988; Fig. 1 of this study). At Pantelleria, Cl abundances are relatively constant, unlike incompatible elements that increase in concentration during magmatic differentiation (Fig. 1). One explanation for this behavior can be inferred from the experiments of Metrich and Rutherford (1992), as shown in Figure 2. Those workers equilibrated pantellerites and other rhyolites with solutions of alkali chloride and H_2O and found that the Cl content of pantellerites remained constant even as the Cl content of the system increased. This occurred as long as the composition of the bulk fluid (vapor + hydrosaline melt) lay within the field of immiscibility for the system NaCl-H_2O (all pressures <160 MPa at 800 °C: Chou, 1987). For example, at 830 °C, the silicate melt contained ~9500 ppm Cl at 50 MPa and ~8500 ppm at 100 MPa. Under those conditions, the Cl content of the silicate melt must have been buffered at constant composition because of the fixed activities of H_2O and NaCl in the two immiscible fluids (Shinohara et al., 1989; Malinin et al., 1989). Therefore, high and constant Cl concentrations in strongly peralkaline magmas are inevitable when they are saturated with immiscible H_2O-NaCl fluids (vapor + hydrosaline melt) in near-surface magma reservoirs.

Evidence for shallow (~2–4 km) pantellerite magma chambers is abundant and includes the formation of calderas during small-volume eruptions, the absence of exotic lithic fragments in volcanic ejecta, and phase equilibrium constraints (Mahood, 1984). Evidence for saturation of pantellerite with respect to two NaCl-H_2O fluids is shown below.

The samples for this study come from two, crystal-poor, glassy lava (obsidian) flows approximately ten thousand years old from Contradas Sciuvechi and Valenza (P32 and P104, respectively: Table 1) of Pantelleria. The units have been described previously by Mahood

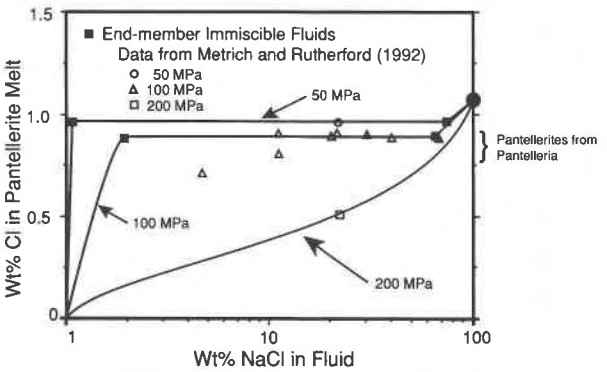

Fig. 2. Cl content of pantellerite melt vs. bulk composition of NaCl-H_2O fluid at 830 °C. The Cl contents of evolved pantellerites from Pantelleria (7500–9000 ppm) are consistent with their having equilibrated at 50–100 MPa with subcritical NaCl-H_2O fluids. At 50 and 100 MPa, Cl concentrations in the melt are fixed as long as the coexisting bulk fluid lies within the field of immiscibility for the system NaCl-H_2O (data from Metrich and Rutherford, 1992). As long as both non-silicate fluids (vapor and hydrosaline melt) are present, their fixed compositions (at a given temperature and pressure) require that the activity, and thus concentration, of Cl in the melt remains constant. At higher pressures, the fluid is supercritical, and any increase in Cl content of the system results in increasing Cl concentration in the melt and fluid (for all fluid compositions). The interpretive curves are based on Shinohara et al. (1989). The compositions of the vapor and hydrosaline melt at 50 and 100 MPa (at 825 °C; from Bodnar et al., 1985) define the pivot points of the curves. The large solid circle represents the Cl content of NaCl-saturated, anhydrous, pantellerite (1.17 ± 0.03 wt%; see Appendix 1).

and Hildreth (1986) and Lowenstern and Mahood (1991). Lowenstern and Mahood (1991) identified two groups of silicate melt inclusions in P32, P104, and other units. Glassy inclusions had degassed prior to or during eruption, usually along narrow capillaries that connect the inclusions to the outside of the host phenocryst, but also along cracks (see also Anderson, 1991). This population of melt inclusions had <1 wt% H_2O, ranging down to <0.2 wt%. Other silicate-melt inclusions were microcrystalline masses of quartz, sanidine, alkali amphibole, and other unidentified phases. When heated in the laboratory at high temperature (825 °C), they melted to hydrous glass (1.8 wt% H_2O for P32 and 2.1 wt% for P104) with a major-element composition equivalent to that of the degassed matrix. Evidently, their higher H_2O contents, relative to glassy, leaked inclusions, promoted crystallization during slow cooling after eruption. All the samples of Lowenstern and Mahood (1991) and Lowenstern et al. (1991) were remelted in a furnace at 1 atm and were observed before and after the experiments (see also Skirius et al., 1990). In the present research, all melt inclusions were originally microcrystalline when selected from phenocryst separates. They were heated in a high-temperature stage attached to a microscope so that they could be observed and photographed.

Table 1. Major-element compositions of whole rocks (WR) and matrix glasses (G) used in this study

Sample*	P32 WR	P32 G	P104 WR	P104 G
SiO_2	69.3	70.3	69.6	71.0
TiO_2	0.36	0.41	0.36	0.42
Al_2O_3	8.18	7.61	8.13	7.41
FeO_{tot}	8.60	9.15	8.71	8.26
MnO	0.29	0.30	0.29	0.30
MgO	0.10	0.11	0.11	0.06
CaO	0.34	0.36	0.35	0.31
Na_2O	6.76	6.81	6.38	6.73
K_2O	4.45	4.59	4.41	4.26
P_2O_5	<0.05	na	<0.05	<0.05
F	0.24	na	0.27	na
Cl	0.77	0.92	0.80	0.88
H_2O	0.28	0.10**	0.43	0.15**
−F, Cl = O	0.55	0.48	0.58	0.47
Total	99.17	100.18	99.31	99.36
Agpaitic index	1.95	2.12	1.94	2.12

* Samples P32 WR and P32 G from Mahood and Stimac (1990). P104 WR from G.A. Mahood (unpublished data) and P104 G from this study. Analytical methods are described in Mahood and Stimac (1990).
** H_2O content of matrix glass from Lowenstern and Mahood (1991).

Volumetric behavior of melt inclusions

Melt inclusions can be understood within the same theoretical and experimental framework that has been developed for other types of fluid inclusions (Hollister and Crawford, 1982; Roedder, 1984). Relative to silicate melt, quartz and most other magmatic phenocrysts are incompressible and inexpansible, and so after entrapment, the inclusion volume is nearly constant (Roedder, 1984). This means that the melt inclusion approximates an isochoric (constant volume) system with $\partial P/\partial T$ equal to the ratio of the coefficient of thermal expansion of the melt (α) to its compressibility (β). Because silicate melts are relatively incompressible, their isochores have relatively steep slopes (6–7 bars/°C for hydrous pantellerite: estimated from data of Lange and Carmichael, 1990), and the internal pressure of inclusions changes rapidly with relatively small changes in temperature (Fig. 3). As long as the quartz host is strong enough to withstand the pressure differential between inclusion and intratelluric melt (Tait, 1992), the pressure in the inclusion is a function of its temperature. When an inclusion-bearing crystal is heated to T_t (its temperature of original entrapment: Table 2), the inclusion should also return to its pressure at the time of entrapment (provided that compressibility of the host is negligible), even if the outside of the phenocryst host is at atmospheric pressure. Therefore, high-temperature heating experiments can recreate the conditions of crystallization in the magma reservoir prior to eruption.

As an inclusion cools below T_t, it will depressurize enough for a shrinkage bubble to nucleate at T_b [compare with Tait (1992), who considers isothermal decompression of melt inclusions]. Once the compressible bubble has formed, the inclusion cools along a curve more shallow than the isochore (the melt-vapor curve of Fig. 3) until the supercooled silicate melt passes through the glass transition at T_g. Additionally, as the inclusion cools to

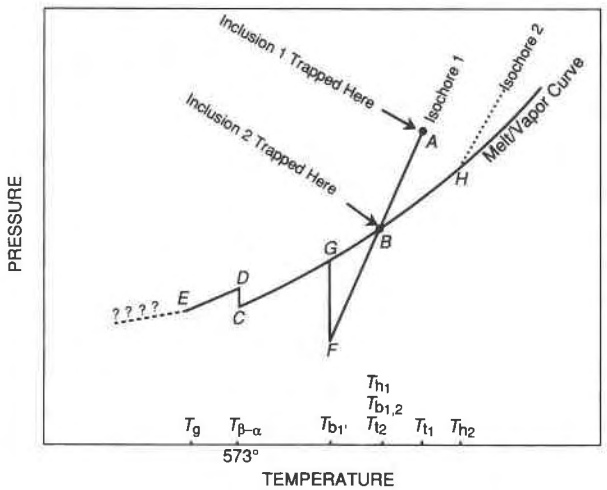

Fig. 3. Schematic pressure-temperature trajectories for three melt inclusions. Inclusion 1, trapping vapor-undersaturated silicate melt at T_{t_1}, cools along Isochore 1 (A to B) until reaching vapor saturation at T_{b_1} and a bubble nucleates. The inclusion cools along the melt-vapor curve (from B to C), and the size of the bubble increases until 573 °C or $T_{\beta-\alpha}$ (C). At C, the quartz host undergoes 1% volumetric contraction, and the inclusion increases in pressure (C to D). The inclusion then cools along a new melt-vapor curve (from D to E) until T_g (E), when the silicate melt passes through the glass transition, and the bubble ceases to grow. Upon heating, the inclusion retraces the same path (E to D to C to B) until bubble and melt homogenize at B (T_{h_1}), and the inclusion joins Isochore 1. An alternative metastable cooling path for Inclusion 1 occurs if a bubble fails to nucleate (so that $T_b < T_h$). The inclusion then cools along its metastable isochore and becomes underpressured, or vapor-supersaturated (B to F), until it reaches $T_{b_1'}$, when the bubble nucleates and equilibrates with the silicate melt (F to G).

Inclusion 2, which trapped two phases, silicate melt + a primary vapor bubble, at T_{t_2} (B), has $T_h > T_t$ because the inclusion must be overpressured to dissolve the extra vapor. In the laboratory, such an inclusion must be heated (from B to H) until the vapor is dissolved at T_{h_2}. Upon further heating, the inclusion follows Isochore 2 (shown as the dotted curve).

room temperature, the internal pressure in the bubble may change as gases condense to their liquid state. At 25 °C, bubbles composed of pure H_2O should have internal pressures equivalent to the vapor pressure of H_2O (0.026 atm). Bubbles with relatively noncondensable gases (e.g., CO_2) retain higher internal pressures at room temperature (up to ~60 atm if liquid CO_2 is absent; Angus et al., 1976).

If a melt inclusion is heated along the melt-vapor curve, its bubble homogenizes into the melt at T_h. Ideally, T_h should be $\leq T_t$. However, some inclusions may contain a vapor bubble that was trapped along with silicate melt (i.e., two phases were trapped). Such inclusions must be brought to higher pressure, by heating above T_t, to dissolve the extra increment of vapor and should have higher homogenization temperatures than inclusions that trapped only silicate melt. In such cases, $T_h > T_t$ (Inclusion 2 in Fig. 3).

Table 2. Notation for describing characteristics of melt inclusions

	Description
T_t	temperature of entrapment of silicate melt inclusion in host phenocryst
T_b	temperature at which bubble nucleates during cooling of silicate melt inclusion
T_g	temperature during cooling at which silicate melt undergoes transition to glassy state
$T_{\beta-\alpha}$	temperature at which quartz undergoes phase transformation (~573 °C at 1 atm)
T_m	temperature, during heating, at which a microcrystalline silicate melt inclusion is converted to silicate melt ± vapor
T_h	temperature, during heating, of homogenization of silicate melt + vapor to a single phase

Analytical techniques

Heating stage experiments

Quartz phenocrysts bearing melt inclusions were doubly polished to provide optimal viewing conditions during high-temperature experiments. Quartz grains were preferred over feldspar because they had significantly less tendency to break during sample preparation and inclusion homogenization. Also, because quartz is the last major phase to crystallize in pantellerite magmas, its inclusions are representative of melt compositions shortly before eruption. Once doubly polished, crystals were typically soaked in acetone to remove mounting resin and impurities. All experiments were done at 1 atm in an H_2O-cooled Leitz 1350 microscope heating stage attached on an Ortholux II Pol-MK microscope with photographic capabilities at the Geological Survey of Japan. Temperature was measured with a $Pt_{87}Rh_{13}$ thermocouple and recorded on a chart plotter. The system was calibrated at the melting temperatures of $K_2Cr_2O_7$ (398 °C), Ag (961 °C), Au (1063 °C), and NaCl (800 °C). Temperature gradients within the sample were negligible because of the small size of individual quartz grains (<1 mm) relative to the sample chamber (1 cm). All samples were analyzed one at a time, and the temperature calibration for each experiment was corroborated by noting the temperature at which vapor bubbles in the inclusions underwent contraction, corresponding to the quartz β to α transition (573 °C). Recorded temperatures are estimated to be accurate to within 15 °C. Typically, inclusions were heated at a rate of 50 °C/min up to a temperature of 600 °C. They were then allowed to equilibrate for 10–20 min before the temperature was raised to 700 °C and they equilibrated for an additional 10 min. The temperature was then raised in 50° increments at 800 °C (again allowing at least 10 min for equilibration at each temperature) and in 25° increments thereafter. Maximum cooling rate for the heating stage was ~400 °/min. All experiments were completed in <3 h.

As discussed below, heating rates may have been too

TABLE 3. Results of heating-stage experiments on Pantellerian melt inclusions

Sample*	T_m (°C)	T_h (°C)	Type**	Opaque crystals?	Inc size (μm)†	Sample	T_m (°C)	T_h (°C)	Type	Opaque crystals?	Inc size (μm)
P32-26	800	940	I or III	No	65 × 75	P32-54.5	850	850	I	Yes	30 × 30
P32-28	850	870	II (1)	Yes	65 × 65	P32-54.6	850	850	I	Yes	30 × 30
P32-29	840	880	II (2)	Yes	60 × 55	P32-56.1	>980	>980	V	—	245 × 100
P32-32.1	<850	860	I	Yes	120 × 120	P32-56.2	885	885	II (3)	Yes	65 × 20
P32-32.2	<850	860	I	Yes	N.R.‡	P32-58	800	890	I	No	240 × 50
P32-32.3	<850	860	I	No	N.R.	P32-59	850	890	I	No	80 × 105
P32-32.4	<850	860	I	No	N.R.	P32-60	780	820	II (3)	Yes	60 × 20
P32-32.5	<850	860	I	No	N.R.	P32-64.1	>850	N.R.	II (1)	Yes	110 × 35
P32-33	930	>930	V	No	N.R.	P32-65.1	800	880	I	Yes	130 × 100
P32-36	950	>950	V	No	N.R.	P32-65.2	850	880	II (1)	Yes	90 × 50
P32-38.1	980	>980	III or V	No	70 × 55	P32-65.3	880	880	II (2)	Yes	40 × 35
P32-38.2	850	870	I	Yes	40 × 30	P32-65.4	850	880	I	Yes	N.R.
P32-38.3	850	870	I	Yes	30 × 20	P32-67.1	800	850	I	No	90 × 90
P32-38.4	850	850	I	No	10 × 10	P32-67.2	850	850	I	No	30 × 25
P32-41.1	860	1200	II (15) + III	No	90 × 60	P32-67.8	880	880	I	No	35 × 35
P32-41.2	810	810	I	No	15 × 15	P32-67.9	850	850	I	No	25 × 20
P32-41.3	810	810	I	No	20 × 20	P32-67.10	880	880	I	No	25 × 20
P32-41.4	810	1100	III	No	15 × 15	P32-73.1	800	870	I	No	90 × 85
P32-46.1	830	880	II (2)	Yes	40 × 30	P32-73.2	850	870	I	No	15 × 15
P32-46.2	830	880	II (1)	Yes	25 × 20	P32-74.1	>900	>900	V	—	240 × 140
P32-49.1	800	875	II (2)	Yes	105 × 60	P32-74.2	900	850	I	Yes	100 × 45
P32-49.2	875	>930	III	No	135 × 90	P32-74.3	850	850	II (2)	No	30 × 30
P32-49.3	800	850	II (1)	Yes	30 × 30	P32-74.4	900	850	II (2)	Yes	50 × 25
P32-49.4	800	850	I	Yes	35 × 35	P32-74.5	850	850	I	No	10 × 10
P32-49.5	800	875	II (3)	Yes	20 × 20	P32-74.6	850	850	I	No	15 × 15
P32-51.1	800	950	III or V	No	75 × 70	P32-77.1	775	850	I	No	150 × 130
P32-51.2	800	930	III or V	No	155 × 50	P32-77.2	775	850	I	No	N.R.
P32-51.3	800	>950	III or V	No	75 × 120	P32-77.3	>850	>850	I	No	N.R.
P32-51.4	800	850	I	No	20 × 20	P32-77.4	>850	>850	I	No	N.R.
P32-51.5	800	850	I	No	35 × 20	P32-77.5	850	850	II (2)	Yes	N.R.
P32-52.1	825	850	I	No	105 × 85	P32-80.1	<850§	<850	II (1)	No	60 × 50
P32-52.2	850	880	II (3)	Yes	20 × 25	P32-80.2	<850§	<850	II (2)	No	40 × 40
P32-52.3	850	880	II (1)	Yes	25 × 10	P32-80.3	<850§	<850	II (2)	No	65 × 45
P32-53.1	>1000	>1000	V	No	105 × 200	P32-80.4	<850§	<850	I	No	80 × 80
P32-53.2	<900	900	I	No	30 × 30	P32-81	<850§	>950	II + III	No	270 × 60
P32-53.3	<900	900	II (1)	No	30 × 40	P104-25	800	830	I	No	150 × 90
P32-54.1	900	>1080	III or V	No	150 × 150	P104-26.1	810	825	I	No	50 × 40
P32-54.2	850	850	II (1)	Yes	30 × 30	P104-26.2	810	825	I	No	55 × 50
P32-54.3	850	850	I	Yes	30 × 30	P104-26.3	810	825	I	No	200 × 55
P32-54.4	850	850	I	Yes	30 × 30						

* Sample number before decimal identifies host crystal. Numbers after the decimal represent multiple inclusions within the same phenocryst.
** Numbers in parentheses indicate number of hydrosaline melt droplets in type II inclusions.
† Inclusion size represents estimate of the longest two dimensions (if inclusion is a parallelepiped). For all inclusions, the third distance (thickness) is intermediate between the two quoted dimensions.
‡ N.R. = not recorded.
§ Inclusions first homogenized in Yamato muffle furnace.

rapid to ensure complete diffusional equilibrium between silicate melt and coexisting vapor bubbles within the time frame of the heating-stage experiments. Therefore, homogenization temperatures listed in Tables 3 and 4 may be 25–75 °C higher than the actual temperatures of inclusion entrapment. Even so, all experiments were conducted in a similar manner, and the recorded data reproducibly identify different populations of inclusions (e.g., one can differentiate Inclusions 1 and 2 of Fig. 3).

Muffle-furnace experiments

Homogenization temperatures were also determined during longer experiments in a Yamato muffle furnace. Unpolished and doubly polished inclusion-bearing quartz grains were placed in a Pt crucible and heated at atmospheric pressure to the experiment temperature at a rate of ~1.25 °C/min. The samples were quenched by removing the crucible from the furnace and cooling it in air. The crucible was cool enough to touch within 2 min, indicating quench rates of ~400 °C/min, similar to those in the heating stage.

Scanning electron microscope (SEM)

Chips of glassy groundmass (~1 mm in diameter) were separated from P32 and soaked in distilled, deionized H_2O to remove any impurities or salts on the glass surface. They were then rinsed in acetone and dried. After the chips were crushed between two clean glass slides, the pantellerite glass shards were sprinkled onto a brass disk coated with wet C paint. The mount was then sprayed with compressed air to remove loose fragments and Au coated. The samples were viewed both with a JEOL 6400 scanning microscope at the Geological Survey of Japan and a Cambridge Instruments 250 Mark II at the U.S.

TABLE 4. Summary of melt inclusion types and their characteristics

Type	T_m (°C)	T_h (°C)*	No. of examples**	Phases present at 900 °C†	Phases at 25 °C after melting experiment	Phases present at T_t (inferred)
I	775–850	825–900	43–44	silicate melt	silicate glass ± shrinkage bubble	silicate melt
II	775–850	825–900	24	silicate melt + hydrosaline melt	silicate glass + (halite + small bubble) ± shrinkage bubble	silicate melt + hydrosaline melt
III	775–850	>950	3–10	silicate melt + vapor	silicate glass + large vapor bubble	silicate melt + vapor
IV	glassy at 25	not studied	—	not studied	degassed silicate glass ± bubble	silicate melt ± vapor: degassed during eruption
V	>1000	>1000	4–8	microcrystalline silicate mass + vapor	microcrystalline silicate mass + vapor	silicate melt ± vapor ± hydrosaline melt: degassed during eruption

* These homogenization temperatures were measured with the heating stage. T_h for group I and II inclusions thus may be 25–75° higher than T_t. Because type III inclusions represent heterogeneous entrapment of magmatic vapor + silicate melt, T_h for them has no real geological significance.

** Some inclusions are classified as more than one type (e.g., II + III) and others are uncertain (e.g., III or V).

† All type I, II, III, and V inclusions contained quartz blebs before, during, and after high-temperature experiments. The small blebs (<20 μm) were apparently refractory daughter crystals that failed to melt during the experiments (see text).

Geological Survey. Mineral phases were identified by using an energy-dispersive detector.

Behavior of Pantellerian inclusions during heating experiments

Table 3 lists the results of all heating-stage experiments performed on melt inclusions in quartz. The data are summarized in Table 4 and below.

Type I: Silicate melt inclusions

Melting of type I inclusions. Upon heating, type I inclusions remained microcrystalline until reaching a temperature between 600 and 700 °C (Fig. 4). At that point, the inclusions became noticeably lighter in color, changing from a dark black-blue to green-gray at the inclusion periphery. With progressive heating, the inclusions continued to melt until they consisted of melt + bubble(s) + quartz, at temperatures ranging from 750 to 850 °C. The temperature at which the inclusion became completely molten (except for quartz and bubbles) is termed T_m. Upon heating above this temperature, the bubble would continue to shrink as the internal pressure in the inclusion increased. All type I inclusions were homogenized to melt + quartz blebs at temperatures ranging from 830 to 900 °C (T_h). Seventy-five percent were homogenized between 850 and 880 °C. When inclusions were homogenized for a second or third time, T_h was usually reproducible to within 25 °C, though the location and number of bubbles produced during cooling varied from experiment to experiment.

The quartz blebs (Fig. 4C) ranged from 5 to 25 μm in size. Because they were also present in all microcrystalline inclusions (unheated) viewed with the SEM or reflecting microscope, the quartz blebs must have grown during original cooling of the inclusions after entrapment (also see Skirius et al., 1990). The quartz blebs never made up more than 5% of the total inclusion volume, and only could be dissolved during long heating experiments (48 h) or at high temperature (>1000 °C). Quartz blebs were not observed in homogenized inclusions in feldspar (J. B. Lowenstern, unpublished data).

Some inclusions contained small opaque grains that did not completely dissolve at T_m. Table 3 notes those inclusions that contained opaque grains, but the T_m listings do not account for their presence, as they usually made up ≪0.1 vol% of the inclusion. In all cases, opaque grains could be dissolved by increasing the temperature to 950 °C for several minutes.

Cooling of type I inclusions. During cooling below T_h, vapor bubbles usually did not nucleate until the inclusion reached 600–700 °C (Fig. 4E); i.e., T_b was as much as 275 °C below T_h. In fact, when cooled at rates of 300–400 °C/min, some inclusions failed to nucleate a bubble. Such phenomena were more common in small inclusions than large ones, though spherical inclusions with diameters of 100 μm usually could be cooled fast enough to produce bubble-free inclusions. Bubble formation and growth was also affected by the quartz β to α phase transition. During some experiments, bubbles would nucleate at temperatures just above 600 °C and would then shrink (or be resorbed) when the quartz host contracted at the β to α phase transition (~573 °C).

Bubbles commonly nucleated on the inclusion wall or on quartz blebs, though many bubbles nucleated within the melt, away from any obvious surface. If more than one bubble formed during the cooling of an inclusion, these bubbles always nucleated simultaneously.

Type II: Silicate melt inclusions with spherical globules (hydrosaline melts)

Heating experiments. Type II inclusions had similar T_m and T_h as type I inclusions, but at temperatures >700 °C, they contained small colorless spherical globules 1–4 μm in size (Fig. 5) of a substance with high optical relief compared with the silicate melt. During heating experiments on microcrystalline inclusions, the globules became visible as the inclusion began to melt, between 650 and 750 °C. During reheating of glassy, previously melted inclusions (more transparent than the microcrystalline inclusions), the features were visible at room temperature as one or more small (<3 μm) colorless cubes and an approximately equal volume of bubble. As the inclusion

was heated above 600 °C, the cube and bubbles homogenized to a single phase: high-relief, spherical globules. Homogenization was complete at temperatures below 700 °C. The globules did not change size during subsequent heating above 700 °C and did not dissolve into the silicate melt even after 30 min at 1000 °C in the heating stage or 48 h at 900 °C in the muffle furnace. There was no correlation between the size of an inclusion and the number of colorless globules within it. If there was more than one inclusion in a phenocryst, a globule might be located in one inclusion, but none would be present in the others. During heating, most globules were not located near vapor bubbles; however, some bubbles apparently contained these small globules within them. At T_h, these bubbles would be resorbed into the silicate melt, leaving only the globule remaining.

As in some type I inclusions, most type II inclusions contained micrometer-sized opaque minerals that melted at temperatures above 900 °C (Table 3 and Fig. 5B) or at lower temperatures (e.g., 800 °C) during longer experiments.

Cooling of type II inclusions. As with type I inclusions, when type II inclusions were cooled below T_h, vapor bubbles would nucleate between 700 and 600 °C, depending on cooling rate. Some vapor bubbles nucleated on spherical globules, though most bubbles formed independently of these features (Fig. 5A).

All globules in type II inclusions crystallized to one or more cubes and an approximately equal volume of bubble at 490 ± 15 °C. This temperature is essentially identical to the 500 ± 10 °C reported by Clocchiatti et al. (1990) for hydrosaline melts within melt inclusions from pantellerites of Montagna Grande on Pantelleria. Bubbles formed by this process never grew >1 μm in size (i.e., they were much smaller than bubbles formed by shrinkage of the silicate melt), presumably because the silicate melt went through the glass transition close to 490 °C (Bacon, 1977), preventing these bubbles from growing. Crystallization of colorless globules was rapid (<1 s). The temperature of crystallization was not affected by the cooling rate of the inclusion, and colorless globules could not be metastably quenched without crystallization, even at cooling rates of 400 °C/min. At room temperature, remnants of the colorless globules consisted of a small bubble and a subequal volume of crystal. The two phases either constituted a sphere (Fig. 5E), or the spherical bubble touched the cubic crystal at one of its corners (Fig. 5D). During the months following the heating-stage experiments, these features changed shape, indicating they were able to equilibrate or recrystallize at room temperature. As discussed in a later section, their composition, thermometric behavior, and crystallization is consistent with that of hydrosaline melts.

Type III: Vapor-rich silicate melt inclusions

This group of inclusions melted to silicate melt + bubbles at similar temperatures as inclusions of types I and II but contained more or larger bubbles than the other types (Fig. 6). Some of these inclusions did not reach T_h, even at 1100 °C. Instead, they consisted of silicate melt + bubbles. Only one bubble was large enough to analyze by FTIR (36 μm), and the analysis showed that the inclusion contained considerable CO_2. Aines et al. (1990) also found CO_2 in several large, Cu-rich bubbles within pantellerite inclusions and interpreted them to be CO_2-bearing vapors present along with silicate melt in the inclusions (i.e., two phases were trapped). After quenching from 900 °C to room temperature, bubbles in these inclusions were sufficiently large that they made up >3 vol% of their host inclusions. Shrinkage bubbles in type I inclusions, even when allowed to equilibrate at 600–700 °C for 20 min, never made up >2 vol% of the inclusion. I interpret type III inclusions as containing one or more magmatic vapor bubbles, as well as silicate melt. Both phases were trapped together in the inclusion at the time of quartz crystallization (Lowenstern et al., 1991). Such a conclusion is consistent with their high homogenization temperatures, the presence of CO_2, and their similar T_m to type I and II inclusions.

Mixed II + III inclusions

Two inclusions contained both hydrosaline melts and large vapor bubbles that homogenized with silicate melt above 950 °C. Both of these inclusions contained more than 15 globules. The globules in P32-81 crystallized to colorless cubes + small (~1 μm) bubbles at 600 ± 10 °C, about 100 °C higher than globules in type II inclusions. P32-41.1 decrepitated at 1100 °C and therefore could not be observed during cooling.

Type IV: Glassy melt inclusions

The group of glassy inclusions was studied by Lowenstern and Mahood (1991: Fig. 1a of that paper) and was shown to have degassed through cracks and narrow capillaries. No additional heating experiments were performed on this population of inclusions.

Type V: Leaked microcrystalline inclusions

Some inclusions could not be melted at temperatures below 1000 °C. Some of these were located near obvious cracks, though no crack was visible near others. These inclusions are interpreted as having partially degassed during or after eruption. Presumably, enough H_2O was left within the inclusion (or cooling was slow enough) to promote devitrification of inclusion glass, and so this class of inclusions may be differentiated from type IV inclusions. Some partially devitrified inclusions, with capillaries visible, appear to be an intermediate class of inclusions between types IV and V.

Muffle-furnace experiments

Several experiments were done in a muffle furnace to assess the effect of time on melting and the homogenization of melt inclusions (Table 5). In one experiment, microcrystalline inclusions were heated for 30 h at 750 °C. Three inclusions (out of 16) melted completely and homogenized to a single melt phase. The cooling rate was evidently fast enough to prevent shrinkage bubbles from

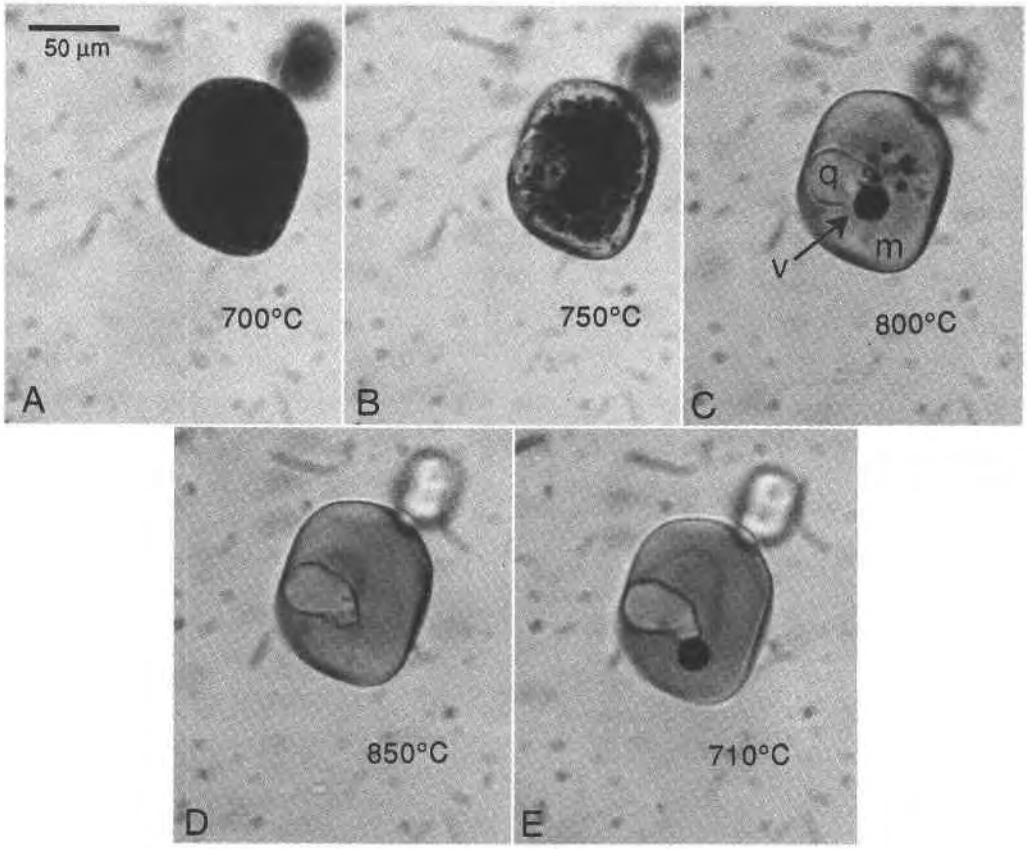
50 µm
700°C
A
750°C
B
q
v
m
800°C
C
850°C
D
710°C
E

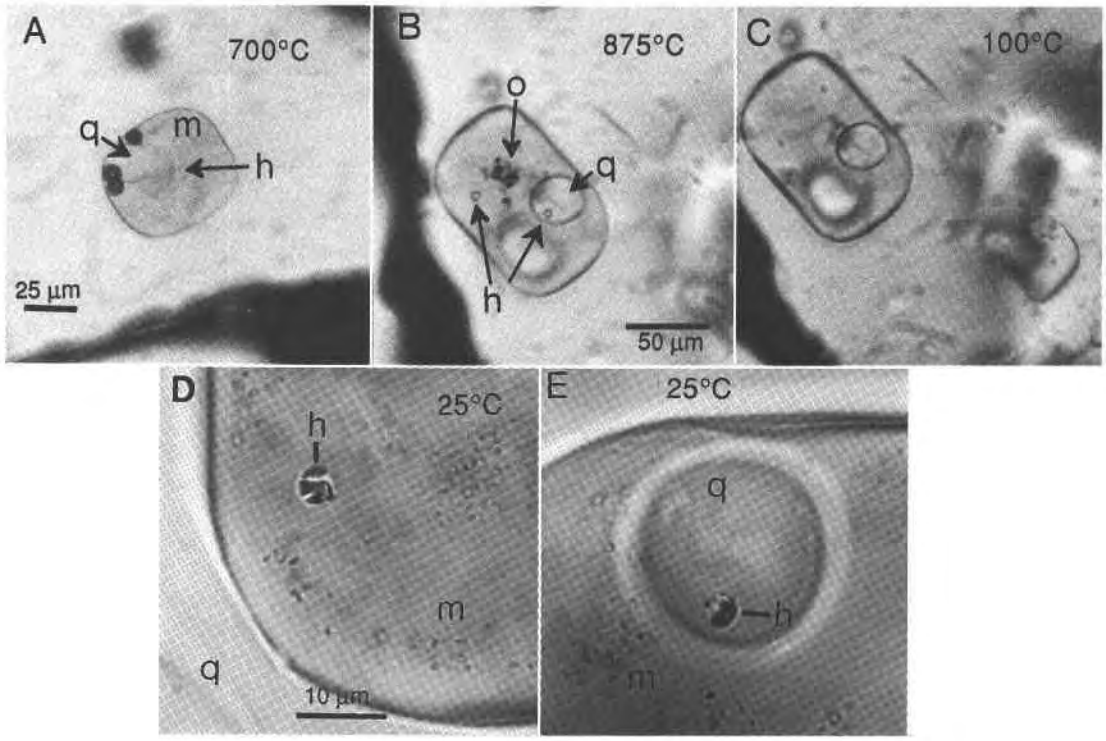
A
700°C
q
m
h
25 µm
B
875°C
o
q
h
50 µm
C
100°C
D
25°C
h
m
q
10 µm
E
25°C
q
h
m

←

Fig. 4. Transmitted light photographs of type I melt inclusion (P32-52; 105 μm in maximum diameter, trapped in quartz) during heating-stage experiment. (**A**) During heating, the inclusion remained microcrystalline until temperatures above 700 °C, when (**B**) melting began around the inclusion periphery. (**C**) At 800 °C, the inclusion had reached T_m and consisted of pantellerite melt (m), refractory quartz (q), and vapor bubbles (v). (**D**) At 850 °C, the inclusion reached T_h, when the bubble was homogenized into the silicate melt. (**E**) During cooling of the inclusion, a vapor bubble nucleated at T_b, which, in this example, was ~140 °C below T_h.

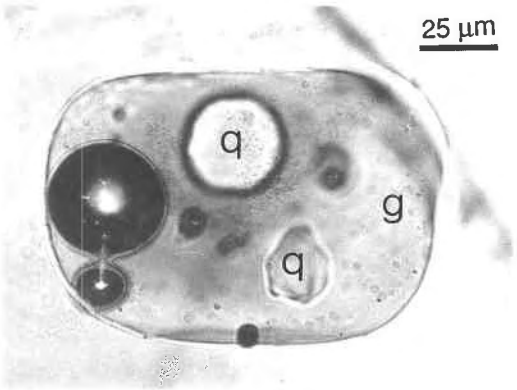

Fig. 6. Transmitted light photograph of type III melt inclusion, P32-49.2 (135 μm in maximum diameter) at room temperature. The inclusion consists of pantellerite glass (g), refractory quartz (q), and five vapor bubbles, two of which are in focus. The inclusion had T_h >930 °C, and the bubbles did not homogenize after 6 h in the muffle furnace at 850 °C. The largest bubble (~39 μm in diameter) contained CO_2, as detected by infrared spectroscopy.

nucleating. Because these inclusions had reached T_h, the experiment apparently indicates that at least some of the inclusions were trapped at temperatures as low as 750 °C, 100 °C lower than the temperatures recorded in most heating-stage experiments. Other inclusions, though, remained partially crystalline. Interestingly, a greater proportion of large inclusions (>50 μm) than small inclusions had reached T_m.

Another experiment showed that the spherical globules in type II inclusions were not resorbed into the silicate melt even after as much as 48 h at 900 °C. Two experiments on type III inclusions showed that the number of bubbles in these inclusions decreased significantly after five or more hours at 850 °C. The remaining bubbles grew larger, though the total volume of bubbles stayed approximately the same. Because the bubbles did not appear to move during these experiments, the growth of large bubbles is likely due to Ostwald ripening rather than the actual coalescence of bubbles.

An experiment on inclusion P32-81 showed that the quartz blebs, present within all inclusions, shrank in size (by about 50%) after 48 h at 900 °C. Additionally, the walls of this inclusion had become more faceted and less rounded. Skirius et al. (1990) discussed faceting in melt inclusions from the Bishop Tuff and concluded that, given sufficient time at high temperature, the walls of melt inclusions will recrystallize to form inclusions with negative crystal shapes (Clocchiatti, 1975). I interpret the quartz blebs in pantellerite melt inclusions in quartz to be daughter products that form during crystallization of the silicate melt to the blue microcrystalline mass. During high-temperature experiments, melting initiates at the inclusion-host border. Partial dissolution of the host might cause the inclusion to become saturated with respect to SiO_2 before all the inclusion contents are melted; as such, no further quartz can be dissolved, and quartz daughter crystals (blebs) remain. However, given sufficient time, the quartz blebs may dissolve and be reprecipitated on the inclusion wall because of the favorable energetics of inclusions with negative crystal shapes.

←

Fig. 5. Transmitted light photographs of type II melt (m) inclusions trapped in quartz. (**A**) Inclusion P32-29 (60 μm in maximum diameter) reached T_b after cooling from T_h. Three bubbles simultaneously formed at 700 °C; none of them nucleated on the white globule (hydrosaline melt droplet; h), though two bubbles nucleated on a refractory quartz bleb (q). (**B**) Two hydrosaline melt droplets (4 μm diameter each) were present within P32-49.1 (105 μm in maximum diameter). During heating, at 875 °C, some opaque crystals (o) remained unmelted but were dissolved above 900 °C. (**C**) During cooling, below 490 ± 15 °C, the hydrosaline melts crystallized and could not be clearly viewed except at 1250× magnification (**D** and **E**, for left and right hydrosaline melts, respectively), which showed them to consist of host glass (m), a vapor (+ liquid?) bubble, and a white crystal with cubic habit (presumably halite). The host crystal was flipped and rotated before photographing **D** and **E**.

Assessment of equilibrium in the laboratory and nature

The reliability of T_h measurements

Data from this study can be used to constrain the temperature of entrapment of silicate melt inclusions to between 750 and 875 °C. Much of this spread appears to be due to real differences in the temperature of entrapment of inclusions. However, several experiments done in the muffle furnace indicated lower T_h for the melt inclusions than experiments using the heating stage. The primary difference between these types of experiments was the time allowed for equilibration. This means that temperatures measured during heating-stage experiments may not reflect the actual T_h because they did not allow sufficient time for diffusion of H_2O between the vapor bubble and silicate melt. The T_h values in Table 3 appear to be between 25 and 75 °C too high, as compared with results shown in Table 5. Similar heating-stage experiments (J. B. Lowenstern, unpublished results) on bubble-bearing melt inclusions from the Valley of Ten Thousand Smokes showed T_h between 25 and 75 °C higher than

TABLE 5. Results of experiments in muffle furnace

Sample	Type	T (°C)*	t (h)**	Description of inclusion before experiment†	Description of inclusion after experiment	Interpreted result‡
P32-26	I	825	4	~70 μm inc: g + large v	g	$T_h < 825$
P32-49.1, 3,5	II, II, II	850	6	90 × 60, 30, and 20 μm incs: all with g + hmr	g + hmr	hydrosaline melt stable at 850
P32-49.2	III	850	6	135 × 90 μm inc: g + ~30 v	g + 2 v	bubbles coalesced at 850; $T < T_h$
P32-51.1	III or V	825	4	75 × 70 μm: g + 1 large v	g + 1 large v	$T_h > 825$ or inc leaked
P32-54	?	850	6	150 × 150 μm inc: g + ~30 v	host crystal cracked and inc vesiculated	Inc leaked
P32-59.1	I	750	30	105 × 80 μm inc: g	g	$T_m < 750$ (?) or silicate melt metastable; v bubble did not nucleate at 750
P32-59.2	I	750	30	35 μm inc: g + x + v	g + v + coarser x	$T_m > 750$
P32-63	I	750	30	60 μm inc, 20 μm inc, 30 μm inc, 20 μm inc, 15 μm inc. All g + x	all incs had g + coarser x	$T_m > 750$; v bubbles do not nucleate at 750
P32-64	I, II	850	5	2 partially melted incs (110 × 35 and 20 × 50 μm)	2 incs with g + x + v: larger inc has hmr	hydrosaline melt stable at 850: T_m and $T_h > 850$ (for both incs)
P32-68	I, I	750	30	1 large (80 × 110 μm) + 1 small (30 μm) micro inc	large inc = g; small inc = g + v + x	large inc: T_m and $T_h < 750$; small inc: $T_m > 750$
P32-69	I, I	750	30	1 large (140 μm) + 1 small (35 μm) micro inc	large inc = g; small inc = v + g + x	large inc: T_m and $T_h < 750$; small inc: $T_m > 750$
P32-70	I, I, I, I	750	30	100 μm inc + 50 μm inc + 40 μm inc + 25 μm inc. All micro incs	100 μm inc = g + v; others = g + v + x	100 μm inc $T_m < 750$; others: $T_m > 750$
P32-71	I, I	750	30	120 × 60 and 50 μm micro incs.	g + v + x	$T_m > 750$
P32-81	II + III	900	48	270 × 60 μm inc: g + >20 v bubbles + hmr + quartz blebs§	g + 3 v + hmr + smaller (by ~50%) quartz blebs	hydrosaline melts stable at 900 and did not coalesce; large v bubbles grew: small bubbles were resorbed. $T_h > 900$; quartz blebs dissolve if given sufficient time

* T = experiment temperature in degrees Celsius.

** t = length of experiment. Time was apparently sufficient to ensure accurate T_m and T_h values.

† Dimensions indicate longest and shortest sides of cylindrical and parallelepiped inclusions or average diameter of spherical inclusions. Values rounded off to nearest multiple of five. All observations were made at room temperature. Abbreviations used: micro = microcrystalline; g = glass; hmr = the products of crystallization of the hydrosaline melts (i.e., micrometer-sized cube + subequal bubble); inc = inclusion; v = vapor bubble; x = silicate or oxide crystals (not quartz blebs).

‡ Unless otherwise stated, T_h was not reached during the experiment (i.e., $T < T_h$). T in degrees Celsius.

§ All inclusions >30 μm in diameter contained small quartz blebs. Those in P32-81 were observed in greater detail.

preeruptive temperatures indicated by iron titanium oxide geothermometry (Hildreth, 1983).

Using solutions provided by Qin et al. (1992) for diffusional exchange between a sphere of radius a (bubble) located within a sphere of radius b (inclusion), one can calculate the time necessary for the attainment of equilibrium. If $a/b = 0.01$, $b = 50$ μm, and the diffusion coefficient for H_2O (or other diffusing species) is 10^{-7} cm^2/s, the system reaches >95% equilibrium in 1.6 min (if the melt-vapor partition coefficient for diffusing species is >0.1). Larger bubbles equilibrate faster than this estimate. A decrease of 1 log unit in the diffusion coefficient increases the time necessary for equilibration by a factor of ten. Above 800 °C, H_2O probably diffuses fast enough to attain equilibrium within the time frame of heating-stage experiments (Karsten et al., 1982). However, because some inclusions appeared to homogenize at lower temperatures during the muffle furnace experiments than in the heating stage, >1 h may be necessary for full equilibration at temperatures below 800 °C. Cl and CO_2, slower diffusing species (Watson, 1991), would reach equilibrium with the bubbles in several tens of minutes to several hours, within the time allotted for the muffle furnace experiments and many of the heating-stage experiments at temperatures above 800 °C.

The major- and trace-element compositions of Pantellerian melt inclusions should become homogeneous within the time scale of most heating-stage experiments. Because the phases within microcrystalline inclusions are very small (<1 μm except for quartz blebs) and appear to have homogeneous distribution, diffusion paths are short, and remelted inclusions should become homogeneous within several tens of minutes.

The control of cooling rate on shrinkage bubble volumes

Besides its strong control on T_b, the cooling rate also affects bubble size. Comparison of the sizes of bubbles in silicate melt inclusions from volcanic rocks may therefore be misleading, unless inclusions with a similar host and

similar size, cooling history, and composition are compared. Comparison of bubble volumes in quartz and plagioclase may be of little value because of the strong effect of the quartz β to α transition on the size of bubbles measured at room temperature. A more reproducible method for comparing sizes of shrinkage or primary bubbles in melt inclusions would be to measure them at nearly magmatic temperatures. Even then, care should be taken to allow sufficient time to eliminate any compositional gradients in the inclusion and to allow the bubble to reach its equilibrium volume.

When cooling rates are very rapid, homogenized inclusions may not nucleate a bubble. Many authors have noted that melt inclusions from crystals in Plinian eruptive products tend not to contain bubbles (e.g., Anderson, 1991; Dunbar and Hervig, 1992; Lowenstern, 1993), whereas those from ignimbrites almost always contain them. Clocchiatti (1972) concluded that crystals from the 1912 ignimbrite of the Valley of Ten Thousand Smokes must have had a relatively slow cooling history because they all contained bubbles. Data from the present study indicate that melt inclusions in hydrous peralkaline rhyolites should not contain shrinkage bubbles if cooled from T_h at rates faster than ~300°/min.

Identification of colorless globules as hydrosaline melts

The behavior of the colorless spherical globules during cooling, including their crystallization to a small cube + bubble around 500 °C, indicates that these features are neither silicate nor oxide phases. Instead, their behavior is consistent with that of hydrosaline melts. They did not homogenize with the silicate melt, even during a 48-h-long experiment at 900 °C (which is above the liquidus; see Appendix 1) and other experiments at lower temperatures, indicating that they represent a separate phase. Their presence in many, though not all, inclusions makes it likely that they were trapped by the quartz along with the silicate melt (i.e., two phases were trapped, which was termed mixed type I-II inclusions by Roedder and Coombs, 1967). The obvious difference in behavior of vapor (shrinkage) bubbles and hydrosaline melts, the fact that these bubbles did not always nucleate on the hydrosaline melts, and the observation that the two phases could touch each other without coalescing indicate that they were not miscible. Furthermore, when coexisting primary (trapped) bubbles and hydrosaline melts were observed, as in P32-81 (a mixed II-III inclusion), the two phases touched each other at temperatures >800 °C and yet did not mix.

The salinity of the hydrosaline melt may be estimated by the temperature at which this phase crystallizes during cooling. If the fluid were an NaCl-H_2O mixture, the crystallization temperature of 490 °C would correspond to the liquidus for a solution with ~60 wt% NaCl (Gunter et al., 1983). However, 490 °C could represent a metastable crystallization temperature if a phase more saline than 60 wt% were supercooled. Therefore, the homogenization temperature of the globules may be more useful toward determining the composition of this phase. During heating experiments, the cube + bubble homogenized to the hydrosaline liquid at temperatures between 600 and 700 °C, liquidus temperatures for solutions with 75–85 wt% NaCl. Therefore, if this phase was an NaCl-H_2O solution, it contained between 60 and 85 wt% NaCl. Though the hydrosaline melt could have contained KCl, $FeCl_2$, or other salts, the high Na and Cl contents of pantellerite make it probable that the phase was mostly NaCl and H_2O. Furthermore, features within outgassed pantellerite matrix, discussed below, appear to corroborate the hypothesis that the cubes within melt inclusions were predominantly halite.

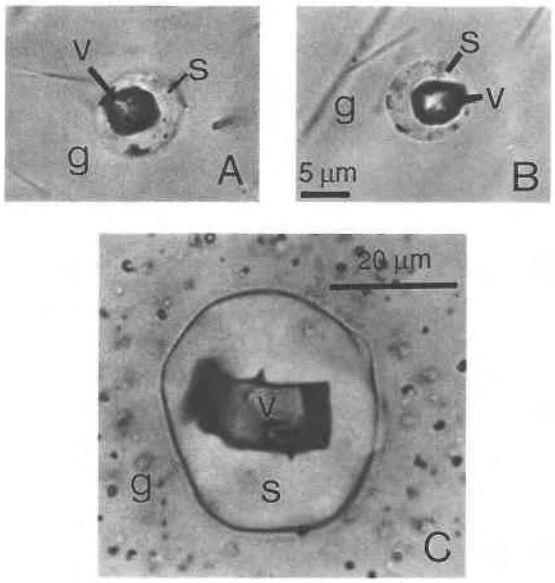

Fig. 7. (**A** and **B**) Transmitted light photographs of fluid inclusions in outgassed pantellerite matrix glass (g) from sample P32. These features (both 9 μm across) consist of a parallelepiped-shaped bubble (v) inside a spherical crystalline shell (s, presumably halite). Several unidentified opaque crystals line the inclusion walls. The inclusions are interpreted to be the crystallized remains of hydrosaline melts. (**C**) Synthetic fluid inclusion (37 μm in diameter), similar to natural inclusions (**A** and **B**), produced by saturating pantellerite melt with a solution of 80% NaCl and 20% H_2O at 200 MPa and 900 °C (see Appendix 1).

Fluid inclusions and halite cubes in outgassed matrix glass

Small (1–10 μm), spherical fluid inclusions were identified in matrix glass of samples P32 (Fig. 7) and P104. In transmitted light, the fluid inclusions of P32 usually appear as spherical droplets with two main phases arranged concentrically. The outside of the sphere consists of a transparent crystalline material that often displays cubic cleavage or habit. Inside the crystalline phase resides a bubble with a spherical to rectangular shape. Sometimes, though, the bubble touches the host glass. In

sample P104, fluid inclusions are ellipsoidal and elongate parallel to flow lineations in the glass, so that the bubble commonly touches the sides of the inclusion (the host glass). Presumably, the bubbles contain liquid as well as vapor, although that could not be verified optically. In all inclusions, the bubble has lower relief than both the crystalline host and silicate glass (n = 1.516), whereas the crystalline material has higher relief than silicate glass (consistent with halite: n = 1.544). Small, submicrometer, opaque crystals could be seen within the inclusions but could not be identified. The inclusions are virtually identical in appearance to synthetic fluid inclusions produced by saturating pantellerite melt with hydrosaline melt (80 wt% NaCl) at high temperature and pressure (Fig. 7C; see Appendix 1). The inclusions could not be homogenized at high temperature because heating above 500 °C caused cracking and further degassing of the host matrix glass. Similar fluid inclusions were not found in phenocrysts from the pantellerites from this study; however, Solovova et al. (1991) reported finding highly saline fluid inclusions (>90 wt% NaCl) in anorthoclase from felsic volcanic rocks of Pantelleria (locality not specified).

In this study, the identification of crystalline material in fluid inclusions was aided by use of the scanning electron microscope (SEM). Small clusters of halite, with and without associated bubbles, were observed in SEM images of crushed matrix glass from sample P32. For example, Figure 8 shows examples of the ~100 halite cubes found in three SEM mounts. Halite was typically found as one to ten small cubes embedded in glass. Commonly, these cubes would be next to a small cavity or bubble (C, D, and F of Fig. 8). Occasionally, no bubble would be visible, as in A, B, G, and H. Other times, groups of cubes would be found in a circular region, with an associated bubble (e.g., E). All features labeled in Figure 8 were verified to contain NaCl by energy-dispersive analysis. No other salts (e.g., KCl) were found in the pantellerite matrix, though not all of the very smallest cubes were analyzed. The abundance of halite-bearing inclusions is estimated at 0.01–0.1 vol% of the rock, meaning that these features contain only 0.6–6.0 wt% of the total Cl in the magma.

Behavior of hydrosaline melts during degassing and eruption

I interpret most of the halite cubes viewed in SEM images (Fig. 8) as corresponding to fragments (or cross sections) of spherical fluid inclusions observed in transmitted light images of matrix glass (Fig. 7). The hemispherical cavities in many SEM images also may correspond to bubbles observed within fluid inclusions such as those shown in Figure 7A and 7B. Because these features are reminiscent of cubes and bubbles formed during crystallization of hydrosaline melts in type II silicate melt inclusions (Fig. 5D), I interpret them to be a related phenomenon. They are the cooled and dehydrated remains of hydrosaline melts present during magma storage in a shallow reservoir. The hydrosaline melt would crystallize to halite + vapor before eruption and extrusion (at pressures of 300–400 bars for a fluid with 50–85 wt% NaCl: Chou, 1987). As long as the magma temperature was <800 °C (the melting temperature of NaCl) during extrusion at the surface, the halite would be solid and nonvolatile.

Not all halite cubes found in the pantellerite matrix may be related to hydrosaline melts. Because the pantellerite melt contained ~2% H_2O prior to eruption, and matrix glass now contains only 0.15 wt% H_2O (Lowenstern and Mahood, 1991), the magma must have vesiculated at some point. The relative scarcity of vesicles in glassy matrix means that either degassing occurred without bubble formation, or, more probably, that bubbles were interconnected as a permeable foam, so that gas could escape to the atmosphere. The consequent loss in vapor pressure would have caused most bubbles to be resorbed or flattened during magma ascent (Eichelberger et al., 1986), leaving a dense obsidian. The vapor exsolved during low-pressure degassing of the magma would contain <0.01 wt% NaCl, because of low solubility of this species in high-temperature low-pressure vapors (Pitzer and Pabalan, 1986). Therefore, most halite crystals in matrix glass probably were not precipitated from exsolving vapor. A few halite crystals, however, were found in some large vesicles (>50 μm) in the pantellerite matrix. Flattening and resorption of such vesicles would cause a cubic, vapor-precipitated halite crystal to be embedded entirely in glass. This may have resulted in features such as A, B, and H in Figure 8. However, most halite crystals are associated with a small bubble (cavity) and are similar in size and aspect to the cubes formed during crystallization of hydrosaline melts found in type II melt inclusions and to spherical fluid inclusions found in the matrix (e.g., C, D, E, F, of Fig. 8). Such a texture would not be expected from the collapse of large, halite-bearing vesicles. In some instances, hydrosaline melts may have served as nucleation sites for vesicles of low-salinity vapor. Such two-phase vesicles would be halite rich, and their collapse might result in features such as G of Figure 8.

The halite itself should not be thought of as phenocrystic because it would have been unstable at magmatic temperature in either the original or the degassed magma. Phenocrystic halite could only exist if the concentration of NaCl in the melt exceeded the solubility of halite in pantellerite. The Cl content of NaCl-saturated, anhydrous, pantellerite is 1.17 ± 0.03 wt% (Fig. 2 and Appendix 1), whereas the Cl contents of melt inclusions (0.87 ± 0.10 wt%) and matrix glass (0.92 ± 0.07 wt%) of P32 and P104 are considerably less (J. B. Lowenstern, unpublished electron microprobe analyses; also see Fig. 1). Any H_2O in the system dilutes the molten salt, lowering the activity of NaCl and making halite precipitation even less likely. Halite, therefore, should be resorbed into the silicate or hydrosaline melt phases of these magmas at high temperatures (>700 °C). I interpret halite crystals in pantellerite matrix to be the crystallized remains of hydrosaline melts present within quenched, metastable glass.

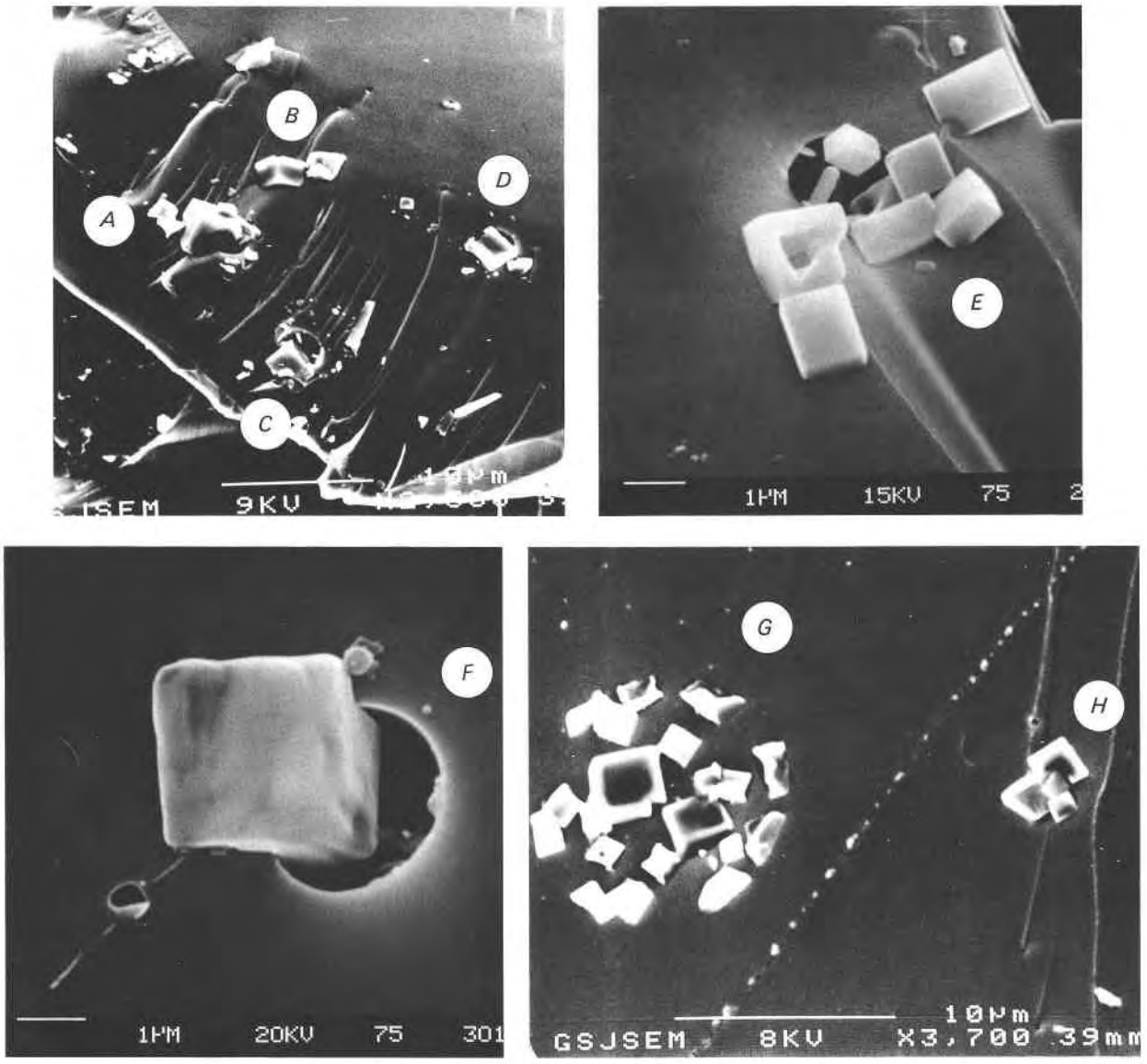

Fig. 8. (A–H) Secondary electron images (with SEM) of halite embedded in naturally outgassed, glassy matrix of pantellerite P32 (an obsidian flow). Many of these crystals are interpreted to be crystallized remnants of hydrosaline melts (Figs. 5 and 7). See text for details.

Immiscible fluids in pantellerites and other magmatic systems

Equilibration depth vs. Cl content of pantellerites

Geological constraints indicate that pantellerite magma chambers may reside at relatively shallow depths (2–6 km) beneath the surface (Mahood, 1984). Information available from pantellerite melt inclusions is consistent with this assertion. Because the glass in pantellerite inclusions contains little CO_2 (Lowenstern and Mahood, 1991), true shrinkage bubbles should contain mostly H_2O. Immiscibility between these H_2O-rich shrinkage bubbles and hydrosaline melts at 800 °C requires that the pressure in the inclusion be lower than 160 MPa, or the two NaCl-H_2O fluids would mix (Chou, 1987). Moreover, the data of Metrich and Rutherford (1992) show that pantellerites equilibrated with vapor and hydrosaline melt at pressures >100 MPa should have lower Cl contents than the units considered here (compare Figs. 1 and 2). This should hold as long as the CO_2 in the system does not strongly affect the solubility of Cl in silicate melt.

The H_2O contents of the pantellerite melt inclusions are also consistent with fractionation at relatively low pressures. Given that the solubility of H_2O in peralkaline melts is about 15% greater than that in metaluminous rhyolites (Webster, 1992b), the 1.8–2.1% H_2O measured in melt inclusions from the pantellerites of this study (Lowenstern and Mahood, 1991) would be consistent with H_2O saturation at 30–40 MPa (Silver et al., 1990). How-

ever, the presence of CO_2-bearing bubbles in type III inclusions indicates that the magma was saturated with a mixed H_2O-CO_2 vapor. As such, the H_2O contents of the melt inclusions would be consistent with vapor saturation at higher pressures (e.g., at 80 MPa, if the vapor contained ~50 mol% H_2O). Lowenstern and Mahood (1991) argued that P32 and P104 were not H_2O saturated because H_2O contents continued to increase with differentiation. It thus appears that these pantellerites equilibrated with a CO_2-bearing vapor and hydrosaline melt at pressures between 50 and 100 MPa. If the solubility of CO_2 in pantellerites is similar to that in metaluminous rhyolites (Fogel and Rutherford, 1990), then the CO_2 contents (<100 ppm) of pantellerites (Lowenstern and Mahood, 1991) are largely consistent with saturation with a mixed H_2O-CO_2 vapor at 50–100 MPa. The strong effect of fluid composition on volatile solubilities makes more quantitative estimates of equilibration pressure highly speculative.

In a similar study of pantellerite melt inclusions from Fantale Volcano, Ethiopia, Webster et al., (1993) found that the peralkaline melt contained higher H_2O contents (4.6–4.9 wt%) and much lower Cl concentrations (0.3–0.4 wt%) than the rocks studied here. If these magmas were H_2O saturated, their H_2O contents would be consistent with fractionation at pressures of 125–145 MPa (Silver et al., 1990). At such pressures and reasonable magmatic temperatures, equilibrium H_2O-NaCl fluids may be supercritical. The relatively low Cl contents of the Fantale pantellerites might then be the result of equilibration of the melt with a relatively Cl-poor fluid and the low fluid-melt partition coefficient for chlorides in peralkaline systems (Webster et al., 1993). Additionally, the low Cl contents may be partially related to the lower FeO_{tot} contents and agpaitic indices of the Fantale glasses relative to the Kenyan pantellerites used by Metrich and Rutherford (1992) and the Pantellerian units studied in this report (Table 1). Those two factors strongly influence the solubility of Cl in silicate melts (Metrich and Rutherford, 1992; Webster, 1992b).

Pantellerites and their high Cl contents

From the above discussion, it is clear that the pantellerite melt had a high Cl concentration because it was buffered by the immiscible vapor and hydrosaline melt. However, this begs the question, how did the Cl content of the system reach levels where the vapor (and silicate melt) could be saturated with hydrosaline melt? The Sr and O isotopic compositions of the pantellerites are inconsistent with incorporation of sea water or melting of sea water–altered crust (Mahood et al., 1990). Apparently, the high Cl abundances are magmatic in nature and can be understood by determining the causes of the high concentrations of a variety of trace elements in pantellerites. Indeed, the concentrations of Cl in pantellerites are only about five to ten times those of most non-degassed metaluminous rhyolites (Dunbar et al., 1989; Westrich et al., 1991; Bacon et al., 1992). This is less than the degree of enrichment of such elements as La, Nb, Zn, and Zr, which have concentrations ten to 25 times those found in metaluminous rhyolites (compare Macdonald and Bailey, 1973; Macdonald et al., 1992). From this perspective, the high Cl concentrations of pantellerites appear more reasonable, and the cause of enrichment will be understood when workers agree on the factors that result in high trace-element concentrations in these rocks.

Do metaluminous rhyolites contain hydrosaline melts?

The solubility of Cl in metaluminous rhyolites is significantly lower than in peralkaline systems (Metrich and Rutherford, 1992; Webster, 1992b). When saturated with immiscible NaCl-H_2O fluids at 100 MPa, these magmas contain about 2700 ppm Cl, as opposed to ~8500 ppm in pantellerites (Metrich and Rutherford, 1992). The lower Cl solubility in metaluminous systems is due to a larger activity coefficient for chloride in the silicate melt, plausibly caused by the lesser number of charge-balancing cations (Na^+, K^+, Fe^{2+}; Webster, 1992b). Although halite-bearing fluid inclusions (e.g., Figs. 7 and 8) have not been reported in metaluminous rhyolitic obsidians, their Cl and H_2O concentrations are typically consistent with hydrosaline melt saturation. Layne and Stix (1991) found that melt inclusions from the Cerro Toledo rhyolites at Valles caldera contained about 2900 ppm Cl and 4.3 wt% H_2O and concluded that these values might indicate saturation with respect to immiscible, subcritical NaCl-H_2O fluids. Many of the silicate melt inclusions saturated with hydrosaline melt described by Frezzotti (1992) also contain similar amounts of Cl. A remarkable number of rhyolites contain 4–5 wt% H_2O and 1700–2100 ppm Cl [e.g., rhyolite from the 1912 Katmai eruption (Westrich et al., 1991; Lowenstern, 1993), Crater Lake climactic eruption (Bacon et al., 1992), and the Taupo rhyolite (Dunbar et al., 1989)]. It is difficult to envision how processes such as crystal fractionation and magma mixing could fortuitously result in such similar volatile concentrations in a variety of silicic magmas. Possibly, the Cl and H_2O concentrations of these rhyolites are controlled by interaction with NaCl-H_2O fluids at shallow crustal depths. If so, peralkaline magmatic systems may only appear to have high Cl contents relative to metaluminous systems because the Cl is partitioned into the melt phase rather than in coexisting fluids. The presence of immiscible NaCl-H_2O fluids in metaluminous porphyry intrusions (Roedder, 1984, chapters 14 and 15) indicates that these magmas eventually become saturated with immiscible NaCl-H_2O fluids.

Degassing of Cl during eruptions: HCl vs. NaCl

Nicholls and Carmichael (1969) argued that the high and relatively constant Cl contents of pantellerites indicated that Cl was not degassed during eruption of these magmas. Because Cl was assumed to be partitioned strongly into exsolving aqueous fluids, they concluded that pantellerites must have low H_2O contents. In actuality,

pantellerites have moderate to high H_2O contents (Kovalenko et al., 1988; Lowenstern and Mahood, 1991; Webster et al., 1993), but the observation of Nicholls and Carmichael (1969) is still valid; Cl appears to be retained in the silicate melt during pantellerite eruptions. The relative nonvolatility of Cl was demonstrated by Webster et al. (1993), who showed that Cl contents of pantellerite melt inclusions from Fantale, Ethiopia, are very similar to those of outgassed matrix. Similar relationships hold at Pantelleria, where Cl appears to be held in the melt during eruption (Kovalenko et al., 1988, 1993). Unpublished data of Lowenstern show an average of 8700 ± 1000 ppm Cl in 12 melt inclusions vs. 9150 ± 770 ppm Cl in matrix glass. This contrasts with metaluminous rhyolites, where matrix glass commonly has lower Cl contents than silicate melt inclusions (e.g., Dunbar et al., 1989; Westrich et al., 1991; Bacon et al., 1992). Because of the low solubility of NaCl in high-temperature H_2O-vapor at low pressure (Pitzer and Pabalan, 1986), no magma is likely to lose significant amounts of NaCl during eruptive degassing. However, HCl, a minor component of magmatic vapors at pressures >50 MPa, increasingly partitions into the vapor (not hydrosaline melt) at low pressure (Shinohara et al., 1984; Shinohara, 1991). Besides pressure, the major factor controlling HCl partitioning between silicate melt and vapor is melt composition. Urabe (1985), in experiments done at 350 MPa, showed that the HCl concentration of magmatic fluid is inversely proportional to the peralkalinity of the coexisting silicate melt. Evidently, metaluminous magma tends to buffer the vapor toward more acidic compositions. This may account for the greater loss of Cl during degassing of metaluminous magmas (as HCl) and the association of H^+ metasomatism (argillic alteration) with shallow calc-alkaline intrusions.

Acknowledgments

Support for this research was provided by the Japanese Agency for Industrial Science and Technology. The data were gathered at the Geological Survey of Japan (G.S.J.); I thank A. Sawaki for offering use of the Leitz 1350 homogenization stage, H. Shinohara for help with the internally heated pressure vessel, and Y. Okuyama for aid with the JEOL 6400 SEM. The manuscript was completed at the U.S. Geological Survey, with support from the National Research Council. Photographic equipment was made available by C.R. Bacon, and R. Oscarson operated the SEM. G.A. Mahood of Stanford University allowed me to use some of her unpublished data, shown in Figure 1 and Table 1, and provided the samples used in this study. Initial study of these samples began while I was supported by N.S.F. grant EAR-8805074 to Mahood. I am grateful for reviews by C.R. Bacon, H. Belkin, G.A. Mahood, E. Roedder, H. Shinohara, and J. Webster. Finally, I am indebted to H. Shinohara for his insightful comments, friendship, and generosity during my stay at G.S.J.

References cited

Aines, R.D., Lowenstern, J.B., and Mahood, G.A. (1990) Evidence for CO_2-rich vapor in pantellerite magma chambers (abs.). Eos, 71 (43), 1699.

Anderson, A.T., Jr. (1991) Hourglass inclusions: Theory and application to the Bishop Rhyolitic Tuff. American Mineralogist, 76, 530–547.

Anderson, A.T., Jr., Newman, S., Williams, S.N., Druitt, T.H., Skirius, C., and Stolper, E. (1989) H_2O, CO_2, Cl and gas in Plinian and ash flow Bishop rhyolite. Geology, 17, 221–225.

Angus, S., Armstrong, B., deReuch, K.M., Altunin, V.V., Gadetskii, O.G., Chapela, G.A., and Rowlinson, J.S. (1976) Interational thermodynamic tables of the fluid state, vol. 3, Carbon dioxide, 385 p. Pergamon, Oxford, England.

Bacon, C.R. (1977) High temperature heat content and heat capacity of silicate glasses: Experimental determination and a model for calculation. American Mineralogist, 277, 109–135.

Bacon, C.R., Newman, S., and Stolper, E. (1992) Water, CO_2, Cl, and F in melt inclusions in phenocrysts from three Holocene explosive eruptions, Crater Lake, Oregon. American Mineralogist, 77, 1021–1030.

Benhamou, G., and Clocchiatti, R. (1976) La thermométrie optique, outil pétrologique: Essai d'utilisation et d'application à l'étude des reliquats magmatiques des phénocristaux de laves hyperalcalines de Pantelleria. Bulletin de la Société Française de Minéralogie et de Crystallographie, 99, 111–116.

Bodnar, R.J., Burnham, C.W., and Sterner, S.M. (1985) Synthetic fluid inclusions in natural quartz. III. Determination of phase equilibrium properties in the system H_2O-NaCl to 1000 °C and 1500 bars. Geochimica et Cosmochimica Acta, 49, 1861–1873.

Chou, I-M. (1987) Phase relations in the system NaCl-KCl-H_2O. III. Solubilities of halite in vapor-saturated liquids above 445 °C and redetermination of phase equilibrium properties in the system NaCl-H_2O to 1000 °C and 1500 bars. Geochimica et Cosmochimica Acta, 51, 1965–1975.

Civetta, L., Cornette, Y., Grisci, G., Gillot, P.Y., Orsi, G., and Requejo, C.S. (1984) Geology, geochronology and chemical evolution of the island of Pantelleria. Geological Magazine, 121, 541–562.

Clocchiatti, R. (1972) Les cristaux de quartz des ponces de la Vallée des Dix Milles Fumées (Katmai, Alaska). Comptes Rendus de l'Académie des Sciences de Paris, 274, 3037–3040.

——— (1975) Les inclusions vitreuses des cristaux de quartz: Etude optique, thermo-optique et chimique: Applications géologiques. Mémoires de la Société Géologique de France, LIV, Mémoire 122, 1–96.

Clocchiatti, R., Massare, D., Metrich, N., Joron, J.L., and Weiss, J. (1990) Glass inclusions in quartz of pumice of Montagna Grande (Pantelleria, Island): Appropriate experimental systems for the study of the physicochemical properties of hyperalkaline magmas. Thirteenth Conference on Earth Sciences Abstracts, Grenoble, 31 (in French).

De Vivo, B., Frezzotti, M.L., and Mahood, G. (1992) Fluid inclusions in xenoliths yield evidence for fluid evolution in peralkaline granitic bodies at Pantelleria (Italy). Journal of Volcanology and Geothermal Research, 52, 295–301.

Dunbar, N.W., and Hervig, R.L. (1992) Volatile and trace element composition of melt inclusions from the Lower Bandelier Tuff: Implications for magma chamber processes and eruptive style. Journal of Geophysical Research, 97, 15151–15170.

Dunbar, N.W., Hervig, R.L., and Kyle, P.R. (1989) Determination of pre-eruptive H_2O, F and Cl contents of silicic magmas using melt inclusions: Examples from Taupo volcanic center, New Zealand. Bulletin of Volcanology, 51, 177–184.

Eichelberger, J.C., Carrigan, C.R., Westrich, H.R., and Price, R.H. (1986) Non-explosive silicic volcanism. Nature, 323, 598–602.

Fogel, R.A., and Rutherford, M.J. (1990) The solubility of carbon dioxide in rhyolitic melts: A quantitative FTIR study. American Mineralogist, 75, 1311–1326.

Frezzotti, M.L. (1992) Magmatic immiscibility and fluid phase evolution in the Mount Genis granite (southeastern Sardinia, Italy). Geochimica et Cosmochimica Acta, 56, 21–33.

Frost, B.R., and Touret, J.L.R. (1989) Magmatic CO_2 and saline melts from the Sybille Monzosyenite, Laramie Anorthosite Complex, Wyoming. Contributions to Mineralogy and Petrology, 103, 178–186.

Gunter, W.D., Chou, I.-M., and Girsperger, S. (1983) Phase relations in the system NaCl-KCl-H_2O. II. Differential thermal analysis of the halite liquidus in the NaCl-H_2O binary above 450 °C. Geochimica et Cosmochimica Acta, 47, 863–873.

Hansteen, T.H. (1989) Fluid and silicate melt inclusions in the Eikeren-Skrim peralkaline granite complex, the Oslo paleorift, Norway. European Current Research on Fluid Inclusions Abstracts, X symposium, London, 45.

Hildreth, W. (1983) The compositionally zoned eruption of 1912 in the

Valley of Ten Thousand Smokes, Katmai National Park, Alaska. Journal of Volcanology and Geothermal Research, 18, 1–56.
Hollister, L.S., and Crawford, M.L., Eds. (1982) Fluid inclusions: Applications to petrology. Mineralogical Association of Canada Short Course Handbook, 6, 304 p.
Karsten, J.L., Holloway, J.R., and Delaney, J.R. (1982) Ion microprobe studies of water in silicate melts: Temperature-dependent water diffusion in obsidian. Earth and Planetary Science Letters, 59, 420–428.
Kovalenko, V.I., Hervig, R.L., and Sheridan, M.F. (1988) Ion microprobe analyses of trace elements in anorthoclase, hedenbergite, aenigmatite, quartz, apatite and glass in pantellerite: Evidence for high water contents in pantellerite melt. American Mineralogist, 73, 1038–1045.
Kovalenko, V.I., Naumov, V.B., and Solovova, I.P. (1993) Behavior of Cl during differentiation and eruption of magmas at Pantelleria. Geochemistry International, 30(7), 105–108.
Lange, R.L., and Carmichael, I.S.E. (1990) Thermodynamic properties of silicate liquids with emphasis on density, thermal expansion and compressibility. In Mineralogical Society of America Reviews in Mineralogy, 24, 25–64.
Layne, G.D., and Stix, J. (1991) Volatile and light lithophile element (LLE) evolution of the Jemez Mountains magmatic system. I. The interval between caldera formation at 1.51 Ma and 1.14 Ma (abs.). Eos, 72(44), 577.
Lowenstern, J.B. (1993) Evidence for a copper-bearing fluid in magma erupted at the Valley of Ten Thousand Smokes, Alaska. Contributions to Mineralogy and Petrology, 114, 409–421.
Lowenstern, J.B., and Mahood, G.A. (1991) New data on magmatic H_2O contents of pantellerites, with implications for petrogenesis and eruptive dynamics at Pantelleria. Bulletin of Volcanology, 54, 78–83.
Lowenstern, J.B., Mahood, G.A., Rivers, M.L., and Sutton, S.R. (1991) Evidence for extreme partitioning of copper into a magmatic vapor phase. Science, 252, 1405–1409.
Luhr, J.F. (1990) Experimental phase relations of water- and sulfur-saturated arc magmas and the 1982 eruptions of El Chichón Volcano. Journal of Petrology, 31, 1071–1114.
Macdonald, R., and Bailey, D.K. (1973) The chemistry of the peralkaline oversaturated obsidians. U.S. Geological Survey Professional Paper, 440-N-1, 37 p.
Macdonald, R., Smith, R.L., and Thomas, J.E. (1992) Chemistry of the subalkalic silicic obsidians. U.S. Geological Survey Professional Paper, 1523, 214 p.
Mahood, G.A. (1984) Pyroclastic rocks and calderas associated with strongly peralkaline magmatism. Journal of Geophysical Research, 89, 8540–8552.
Mahood, G.A., and Hildreth, W. (1986) Geology of the peralkaline volcano at Pantelleria, Strait of Sicily. Bulletin of Volcanology, 48, 143–172.
Mahood, G.A., and Stimac, J.A. (1990) Trace-element partitioning in pantellerites and trachytes. Geochimica et Cosmochimica Acta, 54, 2257–2276.
Mahood, G.A., Halliday, A.N., and Hildreth, W. (1990) Isotopic evidence for the origin of pantellerites in a rift-related alkalic suite: Pantelleria, Italy. International Volcanological Congress Abstracts, September 3–8, 1990, Mainz, Germany.
Malinin, S.D., Kravchuk, I.F., and Delbove, F. (1989) Chloride distribution between phases in hydrated and dry chloride-aluminosilicate melt systems as a function of phase composition. Geochemistry International, 26, 32–38.
Metrich, N., and Rutherford, M.J. (1992) Experimental study of chlorine in hydrous silicic melts. Geochimica et Cosmochimica Acta, 56, 607–616.
Newman, S., Epstein, S., and Stolper, E. (1988) Water, carbon dioxide, and hydrogen isotopes in glasses from the ca. 1340 A.D. eruption of the Mono Craters, California: Constraints on degassing phenomena and initial volatile content. Journal of Volcanology and Geothermal Research, 35, 75–96.
Nicholls, J., and Carmichael, I.S.E. (1969) Peralkaline acid liquids: A petrological study. Contributions to Mineralogy and Petrology, 20, 268–294.
Pitzer, K.S., and Pabalan, R.T. (1986) Thermodynamics of NaCl in steam. Geochimica et Cosmochimica Acta, 50, 1445–1454.
Qin, Z., Lu, F., Anderson, A.T., Jr. (1992) Diffusive reequilibration of melt and fluid inclusions. American Mineralogist, 77, 565–576.
Roedder, E. (1972) Laboratory studies on inclusions in minerals of Ascension Island granitic blocks, and their petrologic significance. Proceedings of COFFI, 5, 129–138.
——— (1984) Fluid inclusions. Mineralogical Society of America Reviews in Mineralogy, 12, 644 p.
——— (1992) Fluid inclusion evidence for immiscibility in magmatic differentiation. Geochimica et Cosmochimica Acta, 56, 5–20.
Roedder, E., and Coombs, D.S. (1967) Immiscibility in granitic melts, indicated by fluid inclusions in ejected granitic blocks from Ascension Island. Journal of Petrology, 8, 417–451.
Shinohara, H. (1991) Pressure dependence of water/rock reaction and control of HCl/NaCl ratio. In Y. Matsuhisa, M. Aoki, and J.W. Hedenquist, Eds., High-temperature acid fluids and associated alteration and mineralization: Report of the Geological Survey of Japan, 277, 97–99.
Shinohara, H., Iiyama, J.T., and Matsuo, S. (1984) Comportement du chlore dans le système magma granitique-eau. Comptes Rendus de l'Académie des Sciences de Paris, 298, 741–743.
——— (1989) Partition of chlorine compounds between silicate melt and hydrothermal solutions. I. Partition of NaCl-KCl. Geochimica et Cosmochimica Acta, 53, 2617–2630.
Silver, L.A., Ihinger, P.D., and Stolper, E. (1990) The influence of bulk composition on the speciation of water in silicate glass. Contributions to Mineralogy and Petrology, 104, 142–162.
Skirius, C.M., Peterson, J.W., and Anderson, A.T., Jr. (1990) Homogenizing rhyolitic glass inclusions from the Bishop Tuff. American Mineralogist, 75, 1381–1398.
Solovova, I., Naumov, V., Girnis, A., Kovalenko, V., and Guzhova, A. (1991) High-temperature fluid heterogeneity: Evidences from microinclusions in Pantelleria volcanics (abs.). Plinius, 5, 206.
Sourirajan, S., and Kennedy, G.C. (1962) The system H_2O-NaCl at elevated temperatures and pressures. American Journal of Science, 260, 115–141.
Tait, S. (1992) Selective preservation of melt inclusions in igneous phenocrysts. American Mineralogist, 77, 146–155.
Tuttle, O.F. (1952) Origin of the contrasting mineralogy of extrusive and plutonic salic rocks. Journal of Geology, 60, 107–124.
Urabe, T. (1985) Aluminous granite as a source magma of hydrothermal ore deposits: An experimental study. Economic Geology, 80, 148–157.
Watson, E.B. (1991) Diffusion of dissolved CO_2 and Cl in hydrous silicic to intermediate magmas. Geochimica et Cosmochimica Acta, 55, 1897–1902.
Webster, J.D. (1992a) Fluid-melt interactions involving Cl-rich granites: Experimental study from 2 to 8 kbar. Geochimica et Cosmochimica Acta, 56, 659–678.
——— (1992b) Water solubility and chlorine partitioning in Cl-rich granitic systems: Effects of melt composition at 2 kbar and 800 °C. Geochimica et Cosmochimica Acta, 56, 679–687.
Webster, J.D., Taylor, R.P., and Bean, C. (1993) Pre-eruptive melt composition and constraints on degassing of a water-rich pantellerite magma, Fantale Volcano, Ethiopia. Contributions to Mineralogy and Petrology, 114, 53–62.
Westrich, H.R., Eichelberger, J.C., and Hervig, R.L. (1991) Degassing of the 1912 Katmai Magmas. Geophysical Research Letters, 18, 1561–1564.

Manuscript received June 14, 1993
Manuscript accepted November 22, 1993

Appendix 1.

Powdered matrix glass from unit P32 was equilibrated at 200 MPa and 900 °C for 95 h. The f_{O_2} was kept close to the Co-CoO buffer. The samples were quenched by turning off power to the internally heated pressure vessel, after which the sample temperature dropped to <400 °C within 5 min. Pantellerite with ~2 wt% added H_2O [that of melt inclusions from P32 (Lowenstern

and Mahood, 1991)] was crystal free after the experiment, indicating that 900 °C is above the liquidus for this sample. The experiment shown in Figure 7C was equilibrated with a solution of 80 wt% NaCl and 20 wt% H_2O (added to the charge as NaCl crystals and deionized H_2O). The glassy product contained approximately 9.5 wt% Na_2O, 0.4% K_2O, 4.4% FeO_{tot}, ~4% H_2O, 6500 ppm Cl, and amounts of other elements similar to those of the starting composition. The loss of K and Fe from the samples was due to the lack of those elements in the added fluid (as salts) and the high fluid to glass ratio (2.5). The NaCl-saturated pantellerite (large solid circle in Fig. 2) was synthesized under similar conditions, and the product contained approximately 9.6 wt% Na_2O, 2.0% K_2O, 7.8% FeO_{tot}, <0.5% H_2O, 11700 ppm Cl, and amounts of other elements similar to those in P32 glass. NaCl was added to the charge as halite (halite to glass ratio = 0.3).